IJAME

Int. J. of Applied Mechanics and Engineering, ???, vol. ???, No. ???, pp. ???-???
DOI: 10.59441/ijame/223942

ANALYSIS OF NONLOCAL FEATURES AND MEMORY PHENOMENA IN THE THERMOELASTIC BEHAVIOR OF MULTILAYERED ANNULAR DISCS EXPOSED TO CONVECTIVE HEAT EXCHANGE

Amaleswari Pipalla[1], V.B. Srinivas[1], S. Thakare[2], N.J. Wange[3] and V.R. Manthena[4*]
[1]Department of Mathematics, School of Engineering, Anurag University, Venkatpur, Medchal, Hyderabad, INDIA
[2]Department of Mathematics, Kavikulguru Institute of Technology and Science, Ramtek, Nagpur, INDIA
[3]Department of Applied Mathematics and Humanities, Yeshwantrao Chavan College of Engineering, Nagpur, INDIA
[4]Department of Mathematics, Priyadarshini Bhagwati College of Engineering, Nagpur, INDIA
*Corresponding Author E-mail: vkmanthena@gmail.com

This study presents an analytical investigation of the thermoelastic behavior of multilayered annular discs incorporating nonlocal and memory-dependent effects through a Caputo fractional heat conduction model. The governing fractional heat conduction equation is formulated with convective boundary conditions and solved using an integral transform technique combined with Laplace inversion. Closed-form expressions for temperature distribution are obtained and subsequently used to evaluate thermally induced resultant moments, deflection, and stress components. Numerical simulations are performed for a three-layered disc composed of copper, zinc, and aluminium to examine the influence of fractional order parameters and material properties. The results reveal that lower fractional orders significantly delay thermal propagation due to strong memory effects, leading to smoother temperature and stress distributions, whereas higher orders approach classical behavior with rapid diffusion and increased structural response. A validation study demonstrates excellent agreement with existing results in the limiting case. The findings highlight the critical role of fractional modeling in accurately predicting thermoelastic responses of multilayered structures, with important implications for advanced engineering applications in aerospace, energy systems, and thermal protection design.

Key words: fractional derivatives, multilayered disc, temperature, thermal stresses.

1. Introduction

Multiple material layers stacked in an axisymmetric configuration, each with unique mechanical and thermal properties, make up multilayered thermoelastic discs. In turbomachinery, pressure vessels, rotating machinery, and other industrial systems where temperature and stress control are critical, these discs play vital functions. With each layer created for distinct functional requirements, the multilayer arrangement maximizes performance under a range of operating situations. The interdependence of heat and elastic effects in materials is referred to as thermoelasticity. Thermal stress is produced when materials expand or compress due to temperature fluctuations. Due to their composite construction, multilayered thermoelastic discs exhibit especially complex behavior. As each layer reacts differently to temperature changes, stress is created at the interfaces between layers, making the thermal-elastic interaction more complex.

Since precise control of temperature-induced stresses and deformations is essential for preserving the structural integrity and functionality of materials, thermoelasticity plays a critical role in both industrial applications and spaceflight research. We now have a much better knowledge of how material qualities and fractional ordering parameters affect the thermomechanical behavior of structures because to recent advances in fractional thermoelastic modeling and the study of functionally graded materials. Thermoelastic heat-responsive materials were studied mathematically [1] for functionally graded thick hollow cylinders. Manthena *et al.* [2, 3] derived an

analytical evaluation of the thermoelastic condition of thick cylindrical structures with non-homogeneous material properties, focusing on radially varying characteristics typical of functionally graded materials (FGMs) and examined how temperature changes might result in thermally induced moments and bending stresses.

The design and analysis of thermosensitive structures have been significantly impacted by recent developments in fractional thermoelasticity, which entails modeling materials with fractional order derivatives. This method makes it possible to comprehend how memory effects and non-local behavior impact materials' thermomechanical responses on a deeper level. It is particularly important for spacecraft constructions that are exposed to extremely high temperatures and for industrial applications that are subjected to cyclic thermal loads. The design of heat-resistant materials for aerospace applications, control of thermally induced deflection and moments in multilayered structures, and ongoing research in thermal stress management in FGMs are all made easier by the flexible framework provided by the use of fractional-order derivatives. Our understanding of thermomechanical responses in materials, particularly under complex situations like nonlocal elasticity, phase delays, and fractional calculus, has been greatly enhanced by developments in thermoelasticity and heat conduction models. The aforementioned works offer a variety of perspectives on how contemporary mathematical techniques, including fractional derivatives and nonlocal theories, can be used to address practical thermoelasticity issues. Abouelregal *et al.* [4] studied thermal characteristics using generalized heat transfer. Atta [5] used Atangana-Baleanu fractional operators and partial elasticity heat diffusion theory to investigate the thermoelastic response of a medium having a spherical hollow. Lamba used a cylindrical-polar coordinate system in [6] to investigate thermoelasticity in a hollow cylinder. A two-temperature Caputo-Fabrizio model was introduced by Abouelregal *et al.* [7] to examine a cylinder under mechanical or thermal stresses with changeable boundaries and material properties. Khavale and Gaikwad [8] investigated the stress profiles of a plate. Lamba [9] investigated memory behavior in a thermoelastic cylinder using analytical and numerical techniques. Lamba [10] used a mathematical solution that includes space- and time-fractional derivatives to investigate the quasi-static thermoelastic behavior of a system.

Saidi *et al.* [11] extended traditional heat transfer models by introducing a new model for time-fractional heat transfer that incorporates phase delays and three fractional-order implications. Singh [12], longitudinal and Rayleigh wave speeds were calculated and shown to show how derivative orders and circular frequency affect these speeds in materials. Impact of distribution of stress and thermoelastic behavior in materials were investigated by Tian *et al.* [13]. Wang *et al.* examined thermoelastic attenuation in a size-dependent microresonator in [14], concentrating on a thin circular plate under thermal stresses. Abouelregal *et al.* [15] provided a quantitative characterization of stress changes due to different heat supplies. Guo *et al.* [16] examined the thermo-hydro-mechanical dynamic link with a fractional structure. Using a fractional framework, Jamal *et al.*'s study [17] examined the mechanical wave propagation in spinning medium. Khader *et al.* used combined analytical and numerical techniques to solve a micropolar thermoelasticity problem for a cylinder in [18]. They successfully modeled non-local effects and memory-dependent behaviors in materials by utilizing Caputo fractional derivatives. References [19-22] studied fractional thermoelastic problems in different slolids. These models avoid the singularities common to conventional fractional models by taking into consideration rate-dependent behaviors and diffusion processes under transitory settings. Heat transport and temperature fields in homogeneous substances were studied by Manthena *et al.* [23]. The thermoelastic vibrations of a spinning microbeam under sinusoidal heating and laser pulse heat sources were modeled by Tiwari *et al.* in [24]. In order to create a distribution law for material properties in the context of shifting heat sources, Zhao *et al.* [25] studied an elastic rod with fluctuating fractional variables and a variable-speed heat source.

Abbas [26] investigated thermal response of a 3-phase lag heat conduction model. In another study, Abbas *et al.* [27] examined photothermal response in a semiconductor medium. The results reveal distinct thermal and mechanical wave propagation behaviors due to the two-temperature effects. Similarly, Alzahrani and Abbas [28] discussed photothermal response with a spherical cavity. Abbas and Othman [29] investigated generalized thermo-microstretch solid, due to thermal relaxation. Carrera *et al.* [30] studied the vibrational characteristics of an axially moving microbeam under the influence of two-temperature effects. Their results show that the motion of the microbeam affects its vibrational modes and frequencies, with the two-temperature model adding further complexity to the analysis. Additionally, several other distinguished scholars have made significant contributions to this area of study, as referenced in [31] to [37]. Nur Alam *et al.* [38] investigation

of ferromagnetic materials. Their findings highlighted distinct differences between damped and undamped wave behaviors under the influence of fractional derivatives. Similarly, Nadeem *et al.* [39] studied nonlinear fractional model, which is crucial for understanding wave dynamics in various contexts. Their results demonstrated that fractional derivatives significantly affect solution profiles, altering wave shapes and propagation characteristics. Verma *et al.* [40] studied heat transfer in annular structures. Kulkarni and Deshmukh [41] investigated the thermoelasticity in annular discs due to temperature variations. Their research highlights how thermal stress distributions are influenced by geometric parameters and material properties. The study reveals that temperature variations across the disc's thickness generate substantial radial and tangential stresses, which could affect the disc's structural integrity during operation. Several authors [42-43] studied different fractional problems. Recent studies [44-52] have further demonstrated the importance of fractional and nonlocal approaches.

Because multilayered thermoelastic discs can withstand both mechanical and thermal loads, they are widely used in engineering applications. These discs are made to resist centrifugal pressures and thermal stresses brought on by high speeds and temperature gradients in rotating machinery, such as turbines and rotors. Additionally, they serve as thermal shields in nuclear and aerospace settings, reducing thermal stress on individual parts by distributing heat over several layers to safeguard delicate components. Additionally, to disperse stress and avoid material breakdown under internal pressure and temperature variations, multilayered discs are used in storage tanks and pressure vessels. These discs are essential to semiconductor devices in microelectronics because they control stress distribution and thermal expansion during repeated cycles of heating and cooling.

It is evident from the survey of the literature that not much research has been done on the thermal properties of multilayered solid objects using a temporal fractional heat transfer equation of the non-local Caputo type. The creation of a model to improve comprehension of thermal behavior in multilayered structures is prompted by this discovered gap. This study seeks to provide a detailed insight into the influence of fractional heat model on thermal performance of these systems by combining interface circumstances. The findings are anticipated to have a significant impact on sectors including electronics, thermal insulation, and aircraft that commonly use multilayered materials. Unlike previous studies such as [44], the present work incorporates convective boundary conditions and evaluates thermoelastic responses (moment, deflection, and stress) in a multilayered annular geometry using a nonlocal Caputo fractional framework, thereby extending the applicability of fractional thermoelastic models.

2. Modeling and solving Heat Conduction Equation (HCE)

Heat equation, including heat source, can be derived using the given equations are as follows [31]:

$$\rho C\frac{\partial T}{\partial t}=-\nabla\cdot q+Q\,, \tag{2.1}$$

$$q=-\lambda\nabla T\,, \tag{2.2}$$

where q – heat flux vector, ρ – density, C – calorific heat, T – temperature, Q – heat source, λ – heat conductivity.

Thermal diffusivity is defined as:

$$\alpha=\lambda/\rho C\,. \tag{2.3}$$

Substituting Eq.(2.2) into Eq.(2.1) gives:

$$\rho C\frac{\partial T}{\partial t}=\nabla\cdot\left(\lambda\nabla T\right)+Q\,. \tag{2.4}$$

The fractional HCE is:

$$\rho C\frac{\partial^{\beta}T}{\partial t^{\beta}}=\nabla\cdot\left(\lambda\nabla T\right)+Q. \tag{2.5}$$

The Caputo fractional derivative of order β and its Laplace transform are [32, 33]:

$$\frac{\partial^{\beta}F(t)}{\partial t^{\beta}}=\frac{1}{\Gamma(H-\beta)}\int_{0}^{t}(t-\tau)^{H-\beta-1}\frac{d^{H}F(\tau)}{d\tau^{H}}d\tau,\quad H-1<\beta<H, \tag{2.6}$$

$$L\left[\frac{\partial^{\beta}F(t)}{\partial t^{\beta}}\right]=s^{\beta}\overline{F}(s)-\sum_{K=0}^{H-1}F^{(K)}\left(0^{+}\right)s^{\beta-1-K},\quad H-1<\beta<H. \tag{2.7}$$

Here s is the Laplace transform parameter.

The spatial domain of the multilayer disc is defined, as shown in Fig.1, by three main ranges: the radial range r, r_{i-1} to $<r_i$, , where i denotes the index of the layer; the angular range θ, 0 to 2π; and the vertical range z, 0 to h. These boundaries outline the geometric constraints within which the thermal behavior of the disc is analyzed. The schematic for the multilayered disc would typically look like concentric rings, each representing a different layer of the disc.

Fractional HCE (FHCE) for a multilayered disc including heat source is [35, 36]:

$$\frac{1}{r}\frac{\partial}{\partial r}\left(r\frac{\partial T_i}{\partial r}\right)+\frac{1}{r^2}\frac{\partial^2 T_i}{\partial\theta^2}+\frac{\partial^2 T_i}{\partial z^2}+\frac{Q_i(r,\theta,z,t)}{\lambda_i}=\frac{1}{\kappa_i}\frac{\partial^{\beta}T_i}{\partial t^{\beta}} \tag{2.8}$$

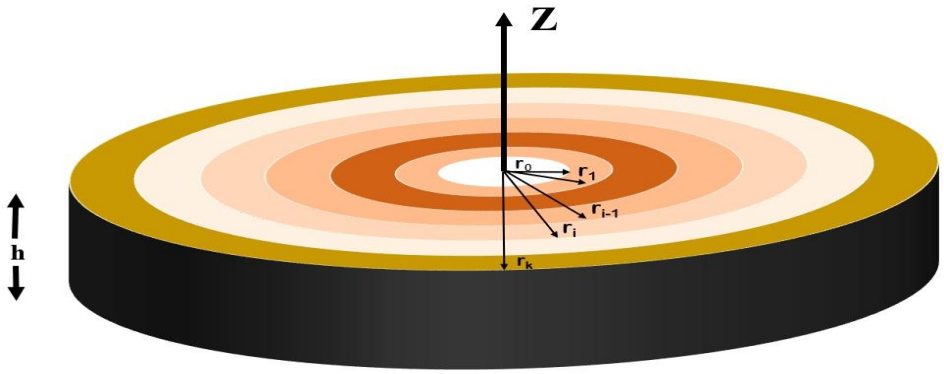

Fig.1. Geometry of the multilayered annular disc.

Boundary and initial conditions:

$$T_i=0,\quad \text{at}\quad t=0,\quad 0<\beta\le 2,$$
$$\frac{\partial T_i}{\partial t}=0,\quad \text{at}\quad t=0,\quad 1<\beta\le 2. \tag{2.9}$$

● Convective boundary on the radial surfaces:

○ At the inner surface $\boldsymbol{r = r_0}$ (inner radius of the disc):

$$\lambda_0 \frac{\partial T_1}{\partial r} + h_0 T_1 = 0, \quad \text{at} \quad r = r_0 , \tag{2.10}$$

where h_0 – heat transfer coefficient at inner radius.

○ At the outer surface $r = r_k$ (outer radius of the disc):

$$\lambda_k \frac{\partial T_k}{\partial r} + h_k T_k = f_k(z, \theta, t), \quad \text{at} \quad r = r_k , \tag{2.11}$$

where h_k – heat transfer coefficient at outer radius.

● Interface conditions between layers:

$$\begin{aligned} &T_i(r_{i-1}, \theta, z, t) = T_{i-1}(r_{i-1}, \theta, z, t), \\ &\lambda_i \frac{\partial T_i}{\partial r}|_{r=r_{i-1}} = \lambda_{i-1} \frac{\partial T_{i-1}}{\partial r}|_{r=r_{i-1}} . \end{aligned} \tag{2.12}$$

● Angular (periodic) boundary conditions:

$$\begin{aligned} &T_i|_{\theta=0} = T_i|_{\theta=2\pi}, \\ &\frac{\partial T_i}{\partial \theta}|_{\theta=0} = \frac{\partial T_i}{\partial \theta}|_{\theta=2\pi} . \end{aligned} \tag{2.13}$$

● Boundary conditions on the top and bottom surfaces:

$$T_i = 0, \quad \text{at} \quad z = 0 \quad \text{and} \quad z = h . \tag{2.14}$$

We use following dimensionless parameters:

$$\begin{aligned} &T_i^* = \frac{T_i}{T_0}, \quad r^* = \frac{r}{h}, \quad \theta^* = \frac{\theta}{2\pi}, \quad z^* = \frac{z}{h}, \quad t^* = \frac{\kappa_1 t}{h^2}, \quad \lambda_i^* = \frac{\lambda_i}{\lambda_0}, \quad \kappa_i^* = \frac{\kappa_i t_0}{h^2}, \\ &\left(r_i^*, h^*\right) = \frac{(r_i, h)}{h}, \quad E_i^* = \frac{E_i}{E_1}, \quad a^* = \frac{a h^2}{\kappa_1}, \quad \varpi_j^* = \frac{\varpi_j h^2}{\kappa_1}, \quad j = 1, 2. \end{aligned} \tag{2.15}$$

The internal heat source $Q_i(r, \theta, z, t)$ and heat flow $f_k(z, \theta, t)$ are given as:

$$Q_i(r, \theta, z, t) = Q_0 Q^*(r^*, \theta^*, z^*, t^*), \quad f_k(z, \theta, t) = f_0 f_k^*(z^*, \theta^*, t^*) . \tag{2.16}$$

Here, Q_0 and f_0 are the dimensional heat source strength and heat flow strength, respectively, $Q^*(r^*, \theta^*, z^*, t^*)$ and $f_k^*(z^*, \theta^*, t^*)$ are dimensionless.

By applying the non-dimensional parameters and variables from Eqs (2.15)-(2.16) to the governing Eqs (2.8)-(2.14), the following dimensionless eqn. is obtained (asterisks omitted for simplicity):

$$\frac{1}{r}\frac{\partial}{\partial r}\left(r\frac{\partial T_i}{\partial r}\right)+\frac{1}{2\pi r^2}\frac{\partial^2 T_i}{\partial \theta^2}+\frac{\partial^2 T_i}{\partial z^2}+P_0 Q_i\left(r,\theta,z,t\right)=P_1\frac{\partial^{\beta} T_i}{\partial t^{\beta}} \tag{2.17}$$

Here, $P_0=\dfrac{Q_0 h^2}{\lambda_i \lambda_0 T_0}$ is a non-dimensional parameter representing the strength of the internal heat source, associated with the Pomerantsev number. Another key parameter, $P_1=\dfrac{t_0\left(\kappa_1\right)^{\beta}}{\kappa_i\left(h^2\right)^{\beta}}$, is also non-dimensional and is related to the fractional time derivative, serving as a modified Kirpichev number.

$$\begin{aligned} &T_i=0, \quad \text{at} \quad t=0, \quad 0<\beta\le 2\ , \\ &\frac{\partial T_i}{\partial t}=0, \quad \text{at} \quad t=0, \quad 1<\beta\le 2, \end{aligned} \tag{2.18}$$

$$\lambda_0\frac{\partial T_1}{\partial r}+Bi_1 T_1=0, \quad \text{at} \quad r=\Phi_1, \tag{2.19}$$

where Φ_1 is the non-dimensional form of r_0, and $Bi_1=\dfrac{h_0 h}{\lambda_0}$ is the Biot number for the inner surface.

$$\lambda_k\frac{\partial T_k}{\partial r}+Bi_2 T_k=Kif_k\left(z,\theta,t\right), \quad \text{at} \quad r=\Phi_2\ , \tag{2.20}$$

where Φ_k is the non-dimensional form of r_k, $Bi_2=\dfrac{h_k h}{\lambda_0}$ is the Biot number for the inner surface, and $Ki=\dfrac{f_0 h}{\lambda_0 T_0}$.

$$\begin{aligned} &T_i\left(r_{i-1},\theta,z,t\right)=T_{i-1}\left(r_{i-1},\theta,z,t\right), \\ &\lambda_i\frac{\partial T_i}{\partial r}|_{r=r_{i-1}}=\lambda_{i-1}\frac{\partial T_{i-1}}{\partial r}|_{r=r_{i-1}}, \end{aligned} \tag{2.21}$$

$$\begin{aligned} &T_i\,|_{\theta=0}=T_i\,|_{\theta=1}, \\ &\frac{\partial T_i}{\partial \theta}|_{\theta=0}=\frac{\partial T_i}{\partial \theta}|_{\theta=1}, \end{aligned} \tag{2.22}$$

$$T_i=0, \quad \text{at} \quad z=0,\ h\,. \tag{2.23}$$

The internal heat source $Q_i(r,\theta,z,t)$ and heat flow $f_k(\theta,z,t)$ are defined as:

$$Q_i(r,\theta,z,t) = q_1\delta(r-r_a)\delta(\theta-\theta_0)\delta(z-z_0)\delta(t),$$

$$f_k(\theta,z,t) = q_2\delta(\theta-\theta_0)\delta(z-z_0)\exp(at).$$

Here, q_1 and q_2 represent the strengths of heat source.

To solve the fractional heat conduction equation (FHCE), several mathematical techniques are employed. A Fourier transform is applied in the z-direction, an eigenfunction expansion is used in the θ-direction (Appendix A), and an integral transform is applied in the *r*-direction (Appendix B). By applying the transformations and reducing the equation, the resulting differential eqn. for the transformed temperature function $\overline{\overline{T}}^{\varphi}_{mp}$ becomes:

$$\frac{d\overline{\overline{T}}^{\varphi}_{mp}}{dt} + A_2\overline{\overline{T}}^{\varphi}_{mp} = A_3\exp(at) + A_4\delta(t), \tag{2.24}$$

where A_2, A_3, and A_4 are constants defined in Appendix B.

Initial conditions:

$$\begin{aligned} &\overline{\overline{T}}^{\varphi}_{mp} = 0, \quad \text{at} \quad t = 0, \quad 0 < \beta \le 2, \\ &\frac{\partial\overline{\overline{T}}^{\varphi}_{mp}}{\partial t} = 0, \quad \text{at} \quad t = 0, \quad 1 < \beta \le 2. \end{aligned} \tag{2.25}$$

To solve the differential Eq.(2.24), Laplace transform and its inversion are applied to obtain:

$$\overline{\overline{T}}^{\varphi}_{mp} = A_3\int_0^t t^{\beta-1}E_{\beta,\beta}\left(-A_2t^{\beta}\right)\exp(a(t-\tau))d\tau + A_4t^{\beta-1}E_{\beta,\beta}\left(-A_2t^{\beta}\right), \tag{2.26}$$

where $E_{\beta,\beta}$ denotes the Mittag-Leffler function.

Finally, by applying the inverse transforms (Appendix C), the temperature distribution in the i-th layer can be expressed as a series solution:

$$\begin{aligned} T_i(r,z,\theta,t) = &\sum_{n=1}^{\infty}\{\sum_{p=1}^{\infty}B_1R_{i0p}(r) + \sum_{m=1}^{\infty}\sum_{p=1}^{\infty}B_2R_{imp}(r)\cos(m\theta) + \\ &+\sum_{m=1}^{\infty}\sum_{p=1}^{\infty}B_3R_{imp}(r)\sin(m\theta)\}\sin(n\pi z/h), \end{aligned} \tag{2.27}$$

where R_{i0p} and R_{imp} are the radial eigenfunctions, and the parameters B_1, B_2, and B_3 are constants determined in Appendix C.

3. Thermoelastic analysis

The equation for symmetrical deflection $w^{(i)}$ of the i-th layer of an annular disc under thermal loads is given by [36, 37]:

$$\nabla^2\nabla^2 w^{(i)} = \frac{-1}{(1-\nu_i)D_i}\nabla^2 M_T^{(i)}. \tag{3.1}$$

In this context, ∇^2 represents the Laplacian operator in cylindrical coordinates which is given by:

$$\nabla^2 = \frac{\partial^2}{\partial r^2} + \frac{1}{r}\frac{\partial}{\partial r} + \frac{1}{r^2}\frac{\partial^2}{\partial \theta^2}. \tag{3.2}$$

The symbol ν_i denotes the Poisson's ratio for the i-th layer. The flexural rigidity of the i-th layer is expressed as $D_i = \frac{E_i h^3}{12\left(1-\nu_i^2\right)}$, where E_i is the modulus of elasticity and h is the thickness of the disc. Additionally, $M_T^{(i)}$ signifies the thermal moment generated by the temperature distribution within the i-th layer. The Laplacian ∇^2 for axisymmetric problems (where the deflection is independent of the angular coordinate θ) is $\nabla^2 = \frac{\partial^2}{\partial r^2} + \frac{1}{r}\frac{\partial}{\partial r} + \frac{1}{r^2}\frac{\partial^2}{\partial \theta^2}$.

The deflection $w^{(i)}$ satisfies the following boundary conditions [36]:

$$w^{(i)} = \frac{\partial w^{(i)}}{\partial t} = 0, \quad \text{at} \quad t = 0, \tag{3.3}$$

$$\frac{\partial w^{(i)}}{\partial r} + w^{(i)} = 0, \quad \text{at} \quad r = r_0, \qquad \frac{\partial w^{(k)}}{\partial r} + w^{(k)} = 0, \quad \text{at} \quad r = r_k,$$
$$w^{(i)} = w^{(i-1)}, \quad \text{at} \quad r = r_{i-1}, \qquad \frac{\partial w^{(i)}}{\partial r} = \frac{\partial w^{(i-1)}}{\partial r}, \quad \text{at} \quad r = r_{i-1}. \tag{3.4}$$

When inline forces are absent, the radial and circumferential forces $N_r^{(i)}$, $N_\theta^{(i)}$, and the shear force $N_{r\theta}^{(i)}$ are zero [37]:

$$N_r^{(i)} = N_\theta^{(i)} = N_{r\theta}^{(i)} = 0. \tag{3.5}$$

The shear forces $Q_r^{(i)}$, $Q_\theta^{(i)}$ are:

$$Q_r^{(i)} = -D_i\frac{\partial}{\partial r}\left(\nabla^2 w^{(i)}\right) - \frac{1}{1-\nu_i}\frac{\partial M_T^{(i)}}{\partial r}, \qquad Q_\theta^{(i)} = -D_i\frac{1}{r}\frac{\partial}{\partial \theta}\left(\nabla^2 w^{(i)}\right) - \frac{1}{1-\nu_i}\frac{1}{r}\frac{\partial M_T^{(i)}}{\partial \theta}. \tag{3.6}$$

The bending moments $M_{rr}^{(i)}$, $M_{\theta\theta}^{(i)}$ are:

$$M_{rr}^{(i)} = -D_i\left[\frac{\partial^2 w^{(i)}}{\partial r^2} + \frac{\nu_i}{r}\frac{\partial w^{(i)}}{\partial r}\right] - \frac{1}{1-\nu_i}M_T^{(i)},$$
$$M_{\theta\theta}^{(i)} = -D_i\left[\nu_i\frac{\partial^2 w^{(i)}}{\partial r^2} + \frac{1}{r}\frac{\partial w^{(i)}}{\partial r} + \right] - \frac{1}{1-\nu_i}M_T^{(i)}. \tag{3.7}$$

Here $M_{rr}^{(i)}$ satisfies the condition:

$$M_{rr}^{(i)}|_{r=r_0} = 0 \quad \text{for all} \quad \theta, \quad 0 < \theta < 1. \tag{3.8}$$

The stress functions $\sigma_{rr}^{(i)}$ and $\sigma_{\theta\theta}^{(i)}$ are:

$$\sigma_{rr}^{(i)} = \frac{1}{h}N_r^{(i)} + \frac{12z}{h^3}M_{rr}^{(i)} + \frac{1}{1-\nu_i}\left(\frac{1}{h}N_T^{(i)} + \frac{12z}{h^3}M_T^{(i)} - \alpha_i E_i T_i\right),$$
$$\sigma_{\theta\theta}^{(i)} = \frac{1}{h}N_\theta^{(i)} + \frac{12z}{h^3}M_{\theta\theta}^{(i)} + \frac{1}{1-\nu_i}\left(\frac{1}{h}N_T^{(i)} + \frac{12z}{h^3}M_T^{(i)} - \alpha_i E_i T_i\right). \tag{3.9}$$

Here, α_i represents the thermal expansion coefficient.

The thermal moment $M_T^{(i)}$ and thermal force $N_T^{(i)}$ are obtained by integrating the temperature distribution over the thickness of the disc:

$$M_T^{(i)} = \alpha_i E_i \int_0^h T_i z dz, \quad N_T^{(i)} = \alpha_i E_i \int_0^h T_i dz \tag{3.10}$$

Using the temperature distribution T_i from Eq.(2.27), the thermal moment $M_T^{(i)}$ is expressed as:

$$M_T^{(i)} = (\alpha_i E_i)\sum_{n=1}^{\infty} B_4\left\{\sum_{p=1}^{\infty} B_1 R_{i0p}(r) + \sum_{m=1}^{\infty}\sum_{p=1}^{\infty} B_2 R_{imp}(r)\cos(m\theta) + \sum_{m=1}^{\infty}\sum_{p=1}^{\infty} B_3 R_{imp}(r)\sin(m\theta)\right\}. \tag{3.11}$$

Similarly, the thermal force $N_T^{(i)}$ is:

$$N_T^{(i)} = (\alpha_i E_i)\sum_{n=1}^{\infty} B_5\left\{\sum_{p=1}^{\infty} D_1 R_{i0p}(r) + \sum_{m=1}^{\infty}\sum_{p=1}^{\infty} B_2 R_{imp}(r)\cos(m\theta) + \sum_{m=1}^{\infty}\sum_{p=1}^{\infty} B_3 R_{imp}(r)\sin(m\theta)\right\}, \tag{3.12}$$

where $B_4 = \left[h^2/\left(n^2\pi^2\right)\right]\left[-n\pi(-1)^n\right]$, $B_5 = \left[h/(n\pi)\right]\left[1-(-1)^n\right]$.

Using Eq.(3.11) in the deflection Eq.(3.1), the radial deflection $w^{(i)}$ is obtained as:

$$w^{(i)} = \left(12\alpha_i\left(1+\upsilon_i\right)/h^3\right)\sum_{n=1}^{\infty}\left\{\left[f_1(r)+f_2(r)\right]^2 / \left[f_1(r)+\left(1+m^2\right)f_2(r)\right]\right\}, \tag{3.13}$$

where: $f_1(r)=\sum_{p=1}^{\infty}B_4B_1\left[a_{i0\,p}J_0(r)+b_{i0\,p}Y_0(r)\right], f_2(r)=\sum_{m=1}^{\infty}\sum_{p=1}^{\infty}B_4B_2\left[a_{imp}J_0(r)+b_{imp}Y_0(r)\right].$

Once the deflection $w^{(i)}$ is obtained, the bending moments $M_{rr}^{(i)}$, $M_{\theta\theta}^{(i)}$, and the stresses $\sigma_{rr}^{(i)}$, $\sigma_{\theta\theta}^{(i)}$ are found using Eqs (3.7) and (3.9) using Mathematica software.

4. Numerical computations

A disc with 3 layers Copper (Cu), Zinc (Zn), and Aluminium (Al) is considered with material properties as shown in Table 1.

Table 1. Physical properties of Copper, Zinc and Aluminium.

Property	**SI Units**	**Copper**	**Zinc**	**Aluminium**
Thermal conductivity	$[W/mK]$	*386*	*113*	*204*
Thermal diffusivity	$\left[m^2/s\right]$	1.11×10^{-4}	0.58×10^{-4}	0.97×10^{-4}
Thermal expansion coefficient	$[1/K]$	16.5×10^{-6}	30.2×10^{-6}	22.5×10^{-6}
Young's modulus	$\left[N/m^2\right]$	11.1×10^{10}	9×10^{10}	7×10^{10}
Poisson's ratio		*0.34*	*0.25*	*0.33*

The numerical simulations utilize several parameters, including an ambient temperature of $T_0 = 293\,K$. The inner radius is set at $r_0 = 1$, the middle radii are $r_1 = 2$ and $r_2 = 3$, and the outer radius is $r_3 = 4$. For the fractional heat conduction equation (FHCE), the specific values of β considered are *0.25* (dotted line), *0.5* (dashed line), *1.5* (thin line), and *2* (thick line).

4.1. Graphical analysis

Figure 2 depicts the temperature distribution across the inner, middle, and outer layers. The main observations from Fig.2 reveal that the temperature starts at zero at the inner radius r_0, aligning with the boundary conditions. In the inner layer (Copper), the temperature rises steadily towards the middle layer, reflecting Copper's high thermal conductivity, which causes a sharp temperature increase. Conversely, the middle layer (Zinc) shows a slight decrease in temperature due to Zinc's lower thermal conductivity, leading to a slower temperature rise and a minor dip in the profile. In the outer layer (Aluminium), the temperature fluctuates; Aluminum's thermal characteristics and the effects of the fractional parameter β create a complex behavior, resulting in non-monotonic temperature changes.

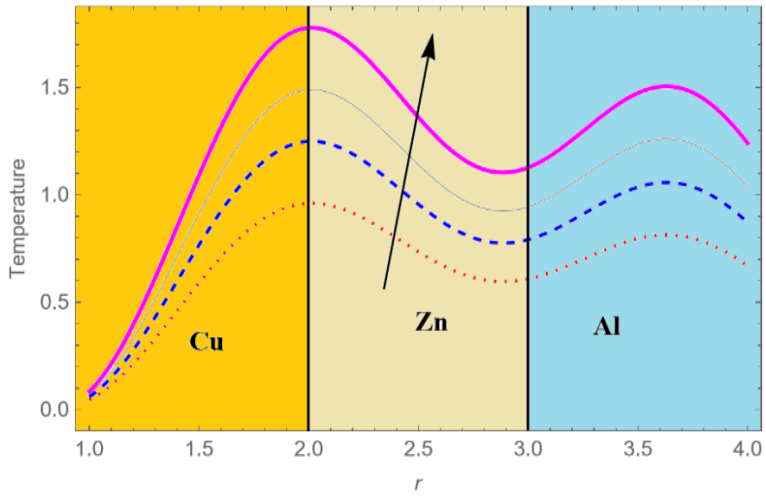

Fig.2. Graph of temperature.

The study concludes, in line with the findings of Ref. [42], that incorporating fractional derivatives into heat transfer analysis significantly improves the understanding of thermodynamics in complex materials. This offers valuable practical implications for engineering applications, particularly in multilayer composite discs.

At the interfaces between layers (Copper-Zinc and Zinc-Aluminium), the temperature profile transitions smoothly, indicating that the conditions of temperature and heat flux continuity are satisfied, despite differing material properties. The impact of the fractional parameter β is evident, with curves plotted for various values (e.g., $\beta = 0.25$, 0.5, 1.5 and 2). The fractional-order values of β directly influence the speed of thermal signal propagation: higher β values result in faster heat diffusion through the layers. For $\beta = 0.25$ (dotted line), the temperature rises slowly due to a strong memory effect, indicating the material retains significant thermal history and causing slower heat propagation. For $\beta = 0.5$ (dashed line), the temperature increase is more rapid, showing a moderate memory effect. The curve for $\beta = 1.5$ (thin line) indicates a much quicker temperature rise, approaching classical heat conduction behavior with reduced memory effects. Finally, for $\beta = 2$ (thick line), this scenario represents classical heat conduction (Fourier heat law), where heat propagates the fastest without memory effects. Thermal signal propagation speeds increase with β, demonstrating that lower β values correlate with slower heat diffusion due to anomalous diffusion behavior, while higher β values approach classical diffusion.

In agreement with the results obtained by Nadeem [39], the findings demonstrate that the generalized fractional-order model provides enhanced accuracy in predicting wave propagation and reflection characteristics in annular spinning discs. The results indicate that incorporating fractional derivatives leads to better alignment with experimental observations and physical phenomena.

Figure 3 demonstrates the deflection behavior of a three-layered annular disc under thermal loads, analyzing the radial deflection across 3 layers. The deflection characteristics are influenced by both the fractional parameters β and the material properties of each layer. The deflection is significantly affected by the material properties, remains stable and consistent as the radius increases. In contrast, the outer layer (Aluminium) exhibits a marked increase in deflection towards the outer boundary due to its lower modulus of elasticity in comparison to other materials.

The fractional parameter β greatly impacts the deflection profile. As β increases, the deflection becomes steeper, suggesting that higher fractional orders facilitate faster heat diffusion, resulting in more significant thermal expansion and larger deflections. The outer layer (Aluminium) shows pronounced deflection as the radius increases, primarily due to its material properties, which include a high thermal expansion coefficient and lower rigidity. In contrast, the deflection in the inner layer (Copper) and middle layer

(Zinc) remains stable across the radial direction due to their higher modulus of elasticity and thermal conductivity, which promote controlled thermal expansion and less variation in deflection. The material properties, including calorific heat, density, and thermal expansion coefficient, contribute to their uniform response to thermal loads.

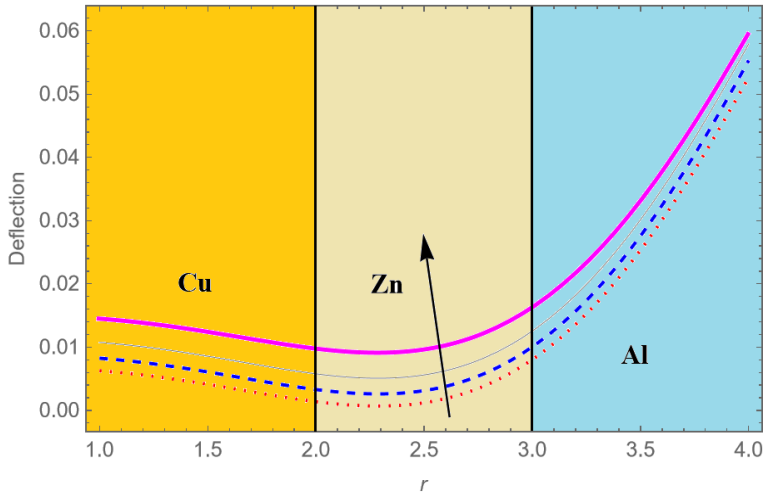

Fig.3. Graph of deflection.

The transitions between layers are smooth, indicating that the boundary conditions at the interfaces (Copper-Zinc and Zinc-Aluminium) are adequately managed. The fractional order parameter β directly influences thermal diffusion rates and, consequently, deflection. Lower β values (e.g., $\beta = 0.25$) result in slower heat diffusion and smaller deflections, while higher values (e.g., $\beta = 1.5$ or $\beta = 2$) lead to quicker thermal responses and sharper deflection profiles. The non-local memory effects associated with lower β values cause deflection to evolve gradually, whereas higher β values result in behavior more akin to classical systems with instantaneous thermal responses, yielding larger deflections, especially in the outer layer. Factors such as calorific heat, thermal expansion coefficient, density, and thermal conductivity play significant roles in this behavior. Lower β values result in slower thermal diffusion and smoother deflection profiles, while higher β values lead to faster heat propagation and sharper deflection profiles.

Figures 4 and 5 represent moments $M_{\theta\theta}$ and M_{rr} in radial direction. These moments are critical for understanding the stress distribution and the structural response of the disc to thermal loads, as they are directly influenced by the material characteristics.

The circumferential moment $M_{\theta\theta}$ starts at zero at the inner radius, which ensures there is no bending moment at the inner boundary of the disc. Increase in Copper layer is observed as one moves radially outward from the inner boundary. Once past the inner layer, $M_{\theta\theta}$ gradually decreases in the intermediate (Zinc) and outer layers (Aluminium). This decline is due to the lower thermal conductivity and modulus of elasticity of these materials compared to Copper, which makes them less capable of sustaining large thermal stresses, resulting in a more gradual reduction of the circumferential moment as the radius increases. As β increases, heat diffusion accelerates, causing larger thermal stresses and greater circumferential moment buildup in the inner layer. Lower values of β lead to a slower moment rise due to stronger memory effects, while higher values result in more rapid increases, indicative of classical heat conduction behavior and faster thermal stress accumulation.

The radial moment M_{rr} experiences an immediate decay in the outer layer (Aluminium) as the radius enters this region. This sharp decrease is due to Aluminium's lower modulus of elasticity and higher thermal expansion coefficient, which allow for easier deformation under thermal loads, leading to a significant reduction in the radial moment. In contrast, the inner layer (Copper) and intermediate layer (Zinc) show non-

uniform variations in the radial moment as the radius increases. The non-uniformity arises from the differing material properties of Copper and Zinc, which react differently to thermal stresses. Copper's higher modulus of elasticity enables it to sustain larger radial moments, while Zinc presents a smoother transition due to its intermediate mechanical properties.

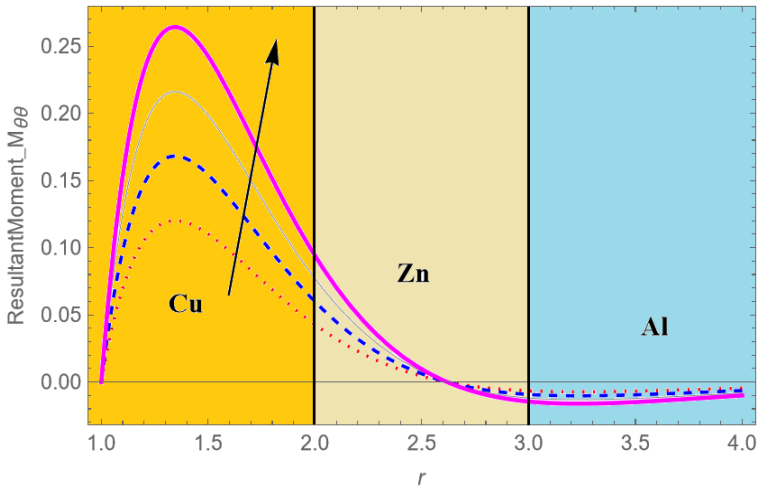

Fig.4. Graph of $M_{\theta\theta}$.

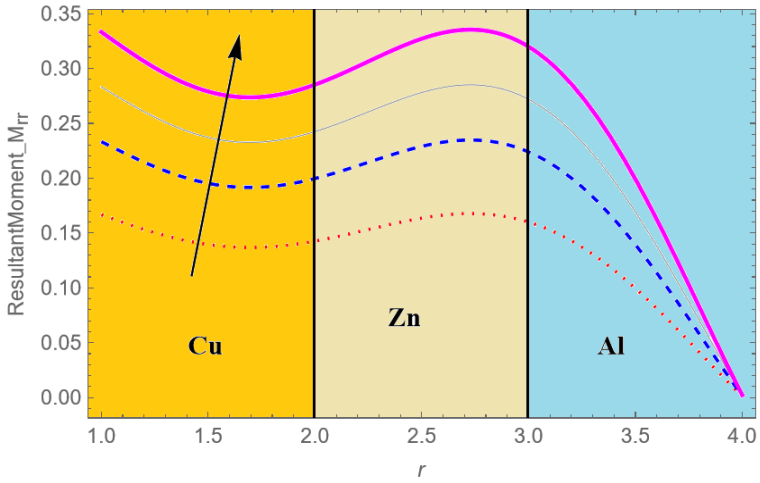

Fig.5. Graph of M_{rr}.

The influence of the fractional parameter β on M_{rr} is notable. Lower β values result in more gradual changes along radial moment, reflecting slower heat diffusion and memory effects typical of fractional heat conduction with smaller β. As β increases, the radial moment becomes more sensitive to thermal stresses, showing larger variations in the inner and intermediate layers. At $\beta = 2$, which represents classical heat conduction, the radial moment peaks more quickly and experiences rapid decay in the outer layer.

The fractional-order parameter β governs heat diffusion rates and the memory effect in the disc's thermal response. Lower β values correspond to slower heat diffusion and larger memory effects, resulting in smoother moment variations, while higher β values lead to faster heat diffusion and greater moments due to rapid thermal stress accumulation. The non-local nature of fractional heat conduction allows for more realistic

modeling of materials where thermal response is influenced by both current and past states. The moments $M_{\theta\theta}$ and M_{rr} reflect the total forces acting on the multilayered disc due to thermal loads, serving as key indicators of the thermal stresses developing within the structure. As seen in [43], the study concludes that the analytical solution provides valuable insights into the temperature distribution in multilayer composite circular discs. The incorporation of fractional calculus enhances the understanding of thermal dynamics in advanced materials, supporting its application in various engineering fields.

Figures 6 and 7 represent stresses, under the impact of various fractional parameters β. The stress distribution is shown along the radial direction, with particular emphasis on the behavior at the interfaces of the distinct material layers and how the fractional-order heat conduction model affects these stress profiles.

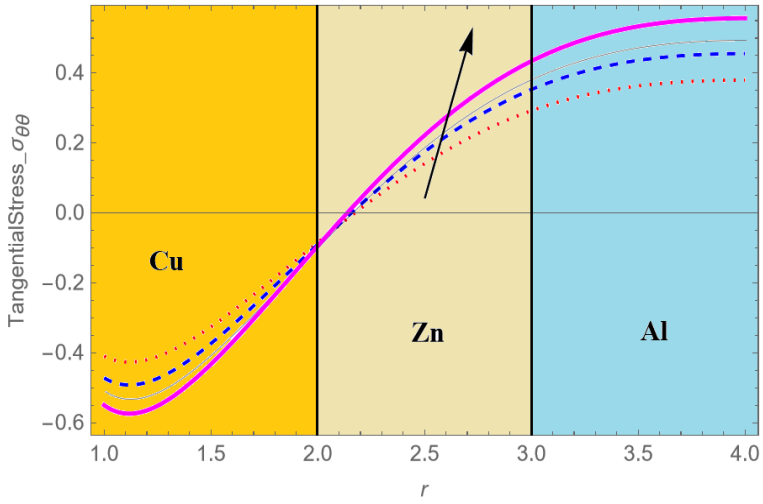

Fig.6. Graph of $\sigma_{\theta\theta}$.

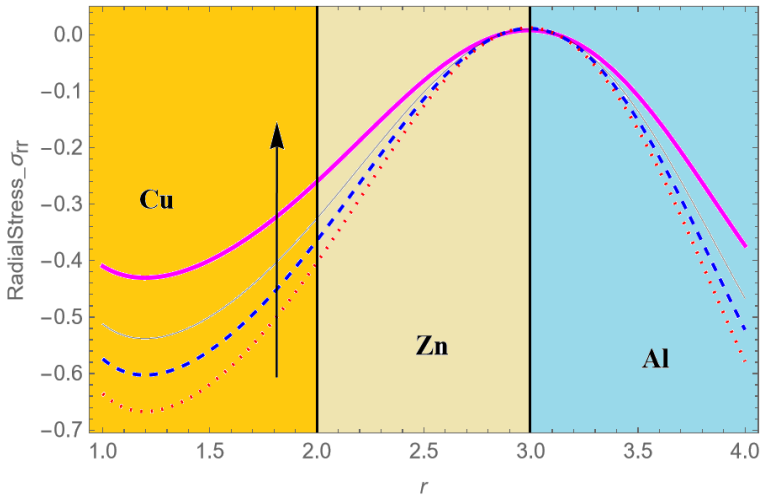

Fig.7. Graph of σ_{rr}.

The radial stress (σ_{rr}) profile exhibits a smooth transition at the interfaces between the different material layers (Copper-Zinc and Zinc-Aluminium), ensuring the continuity of stresses and satisfying boundary conditions. This smoothness is crucial in preventing stress concentrations that could lead to structural failure. In the middle layer (Zinc) and the outer layer (Aluminium), the disc experiences compressive radial stresses, indicative of the materials' tendency to contract under thermal loading. This compressive behavior is

more pronounced in the outer layer due to Aluminium's lower modulus of elasticity and higher susceptibility to deformation under thermal loads. Conversely, the inner layer (Copper) demonstrates a semi-tensile characteristic, where the radial stress σ_{rr} alternates between tensile and compressive states. This behavior arises from Copper's high thermal conductivity and modulus of elasticity, resulting in a rigid response to temperature changes, which allows it to withstand thermal expansion without significant deformation. Lower values (e.g., $\beta = 0.25$) yield a smoother and more gradual stress distribution, reflecting stronger memory effects in the fractional heat conduction model. In contrast, higher values (e.g., $\beta = 1.5$ and $\beta = 2$) result in sharper stress distributions with more pronounced compressive and tensile regions due to faster heat propagation and reduced memory effects.

The tangential stress $\sigma_{\theta\theta}$ begins in a tensile state in the inner layer (Copper), which is expected due to Copper's high thermal conductivity, allowing it to resist contraction under thermal loading. As the radius increases, the tangential stress $\sigma_{\theta\theta}$ gradually rises. In the outermost layer (Aluminium), the tangential stress $\sigma_{\theta\theta}$ transitions to a compressive state as the radius increases, indicating radial contraction under thermal loading. This behavior is linked to Aluminium's lower modulus of elasticity and higher thermal expansion coefficient, making it more susceptible to compressive behavior. Lower β values result in smoother changes, while higher values lead to sharper transitions between tensile and compressive states. At higher β, the tensile stress $\sigma_{\theta\theta}$ in the inner layer increases more rapidly, and the transition to compressive stress in the outer layer occurs more abruptly due to reduced memory effects and faster heat propagation.

The stress behavior in the multilayered disc is significantly influenced by the material properties of each layer. Copper, as the inner layer, exhibits tensile stress due to its high thermal conductivity and resistance to contraction. The middle layer (Zinc) shows a combination of compressive and tensile stresses reflective of its intermediate thermal properties, while the outer layer (Aluminium) experiences compressive stress due to its low elastic modulus and higher thermal expansion coefficient. The fractional-order parameter β is crucial in determining the rate of heat diffusion and the resulting stress distribution. Lower β values correspond to slower heat diffusion and stronger memory effects. Despite the differences in material properties, the smooth transitions in both radial and tangential stresses at the interfaces indicate that continuity conditions for stress and heat flux are met. This continuity is vital for the structural integrity of the multilayered disc, as stress discontinuities could result in material failure at the interfaces.

The obtained results are in good agreement with previously reported studies on fractional and nonlocal thermoelasticity. In particular, the delayed thermal propagation and smooth stress variations at lower fractional orders are consistent with the findings of Tian *et al.* [13] and Li *et al.* [19], where memory effects significantly influence thermal diffusion. Similarly, the rapid increase in temperature and deflection at higher fractional orders aligns with classical thermoelastic behavior reported by Wang *et al.* [14]. The attenuation of displacement and gradual stress transitions observed in the present study further confirm the physical realism of the fractional model, as also discussed in [42]. This comparison demonstrates the reliability and improved predictive capability of the proposed formulation.

5. Limiting case

To verify the correctness of the present formulation, the model is examined in the limiting case when the fractional order parameter approaches unity ($\beta \to 1$), where it reduces to the classical heat conduction model. The obtained results exhibit excellent agreement with the well-established behavior reported in the literature, thereby confirming the accuracy and reliability of the present analytical approach. For $\beta = 1$, the FHCE reduces to the classical heat conduction equation. In this limiting case, the system behaves according to the Fourier law of heat conduction, with no memory effects or non-local influences. This corresponds to a situation where the heat conduction process no longer exhibits memory effects or non-locality in time, and the system follows Fourier law. The graphical analysis from Figures (2) to (7) fits well with the classical heat conduction results in [36] when the fractional parameter $\beta = 1$. This limiting case corresponds to standard heat

conduction with no fractional or memory effects. When the fractional order is taken as one and the second-order axial temperature gradient is ignored, the resulting temperature distribution coincides with the findings reported in [40]. Likewise, for a single-layer circular disk under steady-state conditions, assuming no internal heat generation and neglecting the second-order angular temperature variation, the obtained temperature profile is consistent with the results presented in [41].

6. Conclusion

In this work, a non-local Caputo temporal FHCE for a multilayered thin annular disc is analytically solved using the integral transformation approach, taking into account convection in addition to a number of other constraints. The analysis correctly calculates the thermally induced resultant moments and thermal deflection in addition to deriving the temperature distribution. It also evaluates the stress components numerically. The model allows for a detailed understanding of temperature behavior, resultant moments, and thermal stresses for computational applications by assuming a three-layer annular disk. The following is a summary of the main conclusions:

- Thermal signal propagation is strongly governed by fractional order, where lower values produce delayed diffusion due to memory effects, while higher values approach classical behavior.• Deflection is significantly influenced by both material properties and fractional parameters, with higher fractional orders leading to increased structural deformation.
- Resultant moments exhibit strong sensitivity to fractional order, indicating their importance in thermo-mechanical design considerations.
- Stress distributions reveal smooth transitions across interfaces, confirming continuity conditions and structural stability of multilayered configurations.

In conclusion, the incorporation of fractional-order concepts into multilayered thermoelastic models offers significant potential for enhancing the efficiency and reliability of industrial and aerospace structures. By accounting for fractional heat transfer effects and their influence on thermal stresses, deflections, and bending moments, engineers can develop optimized designs that minimize deformation and prevent structural failure under thermal loading. This approach is especially valuable in engineering fields such as energy systems, automotive engineering, and aerospace technology, where precise thermal and mechanical performance is essential.

Practical implications

From an engineering perspective, the nonlinear thermoelastic response observed under varying fractional parameters has significant implications for design safety and operational limits. Higher fractional orders, which correspond to faster heat propagation, may induce larger thermal stresses and deflections, potentially reducing structural safety margins. In contrast, lower fractional orders introduce memory effects that delay thermal response, thereby reducing peak stresses and improving resistance to thermal shock. These findings are particularly relevant for the design of multilayered components in aerospace and high-temperature environments, where controlled thermal behavior is essential for structural integrity.

Acknowledgment

The authors express their sincere appreciation to the Editor-in-Chief and the esteemed reviewers for their valuable feedback and insightful suggestions, which have significantly enhanced the quality of this manuscript.

Nomenclature

E_i – modulus of elasticity

$C_i(T_i)$ – heat capacity

D_i – flexural stiffness

h – thickness

h_0, h_K – convective heat transfer coefficient

$M_{rr}^{(i)}, M_{\theta\theta}^{(i)}$ – resultant moments

$M_T^{(i)}$, $N_T^{(i)}$ – moments

$N_{rr}^{(i)}, N_{\theta\theta}^{(i)}, N_{r\theta}^{(i)}$ – net forces

$Q(r,\theta,z,t)$ – heat source

$Q_{rr}^{(i)}, Q_{\theta\theta}^{(i)}$ – shear forces

T_i – temperature

T_0 – surrounding temperature

$w^{(i)}$ – deflection

$\alpha_i(T_i)$ – thermal expansion coefficient

$\lambda_i(T_i)$ – heat conductivity

v_i – Poisson's ratio

ρ_i – density

σ_{rr}, $\sigma_{\theta\theta}$ – stresses

Appendix A

By applying Fourier-transform and eigenfunction expansion to the governing equation (2.17) and the boundary conditions (2.22) and (2.23), we obtain the following equation for the temperature distribution:

$$\left(\frac{\partial^2 \overline{\overline{T}}_{im}}{\partial r^2} + \frac{1}{r}\frac{\partial \overline{\overline{T}}_{im}}{\partial r} - \frac{m^2}{2\pi r^2}\overline{\overline{T}}_{im} - \psi_n^2 \overline{\overline{T}}_{im} \right) + P_0 \overline{\overline{Q}}_{im}(r,t) = P_1 \frac{\partial^\beta \overline{\overline{T}}_{im}}{\partial t^\beta} . \tag{A.1}$$

The boundary and initial conditions (2.18) to (2.21) are transformed as follows:

$$\begin{aligned} &\overline{\overline{T}}_{im} = 0, \quad \text{at} \quad t = 0, \quad 0 < \beta \le 2, \\ &\frac{\partial \overline{\overline{T}}_{im}}{\partial t} = 0, \quad \text{at} \quad t = 0, \quad 1 < \beta \le 2, \end{aligned} \tag{A.2}$$

$$\lambda_0 \frac{\partial \overline{\overline{T}}_{1m}}{\partial r} + Bi_1 \overline{\overline{T}}_{1m} = 0, \quad \text{at} \quad r = \Phi_1 , \tag{A.3}$$

$$\lambda_k \frac{\partial \overline{\overline{T}}_{km}}{\partial r} + Bi_2 \overline{\overline{T}}_{km} = Ki \overline{\overline{f}}_{km}(t), \quad \text{at} \quad r = \Phi_2 , \tag{A.4}$$

$$\overline{\overline{T}}_{im}\left(r_{i-1},\theta,z,t\right)=\overline{\overline{T}}_{i-1,m}\left(r_{i-1},\theta,z,t\right),\qquad \lambda_i\frac{\partial\overline{\overline{T}}_{im}}{\partial r}|_{r=r_{i-1}}=\lambda_{i-1}\frac{\partial\overline{\overline{T}}_{i-1,m}}{\partial r}|_{r=r_{i-1}}. \tag{A.5}$$

These expressions include the internal heat source and the external heat flux:

$$\psi_n=n\pi/h,\overline{\overline{Q}}_{im}\left(r,t\right)=\left[\left(q_1\theta_0 z_0\right)/\left(P_0\right)\right]\sin(m\theta_0/2)\sin(n\pi z_0/h)\delta\left(r-r_a\right)\delta\left(t\right),$$

$$\overline{\overline{f}}_{km}\left(t\right)=q_2KiA_1\exp(at),A_1=\theta_0 z_0\sin(m\theta_0/2)\sin(n\pi z_0/h).$$

Appendix B

Applying the integral transform in the radial direction to equation (A.1), we operate on the equation by multiplying it by $rR_{im}\left(r\right)$ and integrating over $[\,r_{i-1}\,,\ r_i\,]$:

$$\begin{aligned}&\int_{r_{i-1}}^{r_i}\left(\frac{\partial^2R_{im}\left(r\right)}{\partial r^2}+\frac{1}{r}\frac{\partial R_{im}\left(r\right)}{\partial r}-\frac{m^2}{2\pi r^2}R_{im}\left(r\right)-\psi_n^2R_{im}\left(r\right)\right)r\overline{\overline{T}}_{im}dr+\\&+\left[rR_{im}\left(r\right)\frac{\partial\overline{\overline{T}}_{im}}{\partial r}-r\overline{\overline{T}}_{im}\frac{\partial R_{im}\left(r\right)}{\partial r}\right]_{r_{i-1}}^{r_i}+\int_{r_{i-1}}^{r_i}\overline{\overline{Q}}_{im}\left(r,t\right)rR_{im}\left(r\right)dr=\ .\\&=\int_{r_{i-1}}^{r_i}\left(P_1\frac{\partial^\beta\overline{\overline{T}}_{im}}{\partial t^\beta}\right)rR_{im}\left(r\right)dr.\end{aligned} \tag{B.1}$$

The function $R_{im}\left(r\right)$ is chosen to satisfy the following radial eigenfunction equation:

$$\frac{\partial^2R_{im}\left(r\right)}{\partial r^2}+\frac{1}{r}\frac{\partial R_{im}\left(r\right)}{\partial r}+\left(-\frac{m^2}{2\pi r^2}-\psi_n^2+\gamma_{im}^2\right)R_{im}\left(r\right)=0\,. \tag{B.2}$$

The boundary and interface conditions for $R_{im}\left(r\right)$ are:

$$\lambda_0\frac{dR_{1m}}{dr}+Bi_1R_{1m}=0\,, \tag{B.3}$$

$$\lambda_{km}\frac{dR_{km}}{dr}+Bi_2R_{km}=0\,, \tag{B.4}$$

$$R_{im}\left(r_{i-1}\right)=R_{i-1,m}\left(r_{i-1}\right),\qquad \lambda_i\frac{dR_{im}}{dr}|_{r=r_{i-1}}=\lambda_{i-1}\frac{dR_{i-1,m}}{dr}|_{r=r_{i-1}}. \tag{B.5}$$

The solutions for $R_{im}\left(r\right)$ are expressed in terms of Bessel functions J_0 and Y_0:

$$R_{imp}\left(\gamma_{imp}r\right)=a_{imp}J_0\left(\gamma_{imp}r\right)+b_{imp}Y_0\left(\gamma_{imp}r\right).$$

After simplification, the integral equation for temperature becomes:

$$\sum_{i=1}^{k}P_0\left[rR_{imp}\left(r\right)\frac{\partial\overline{\overline{T}}_{im}}{\partial r}-r\overline{\overline{T}}_{im}\frac{\partial R_{imp}\left(r\right)}{\partial r}\right]_{r_{i-1}}^{r_i}+\sum_{i=1}^{k}\int_{r_{i-1}}^{r_i}\overline{\overline{Q}}_{im}\left(r,t\right)rR_{imp}\left(r\right)dr=$$
$$=\sum_{i=1}^{k}\int_{r_{i-1}}^{r_i}P_1\left(\frac{\partial^{\beta}\overline{\overline{T}}_{im}}{\partial t^{\beta}}+\kappa_1\gamma_{1mp}^2\overline{\overline{T}}_i\right)rR_{imp}\left(r\right)dr, \tag{B.6}$$

we define:

$$\overline{\overline{T}}_{mp}^{\varphi}=\sum_{i=1}^{k}P_1\int_{r_{i-1}}^{r_i}rR_{imp}\left(r\right)\overline{\overline{T}}_{im}dr,\qquad \overline{\overline{Q}}_{mp}^{\varphi}=\sum_{i=1}^{k}\int_{r_{i-1}}^{r_i}\overline{\overline{Q}}_{im}\left(r,t\right)rR_{imp}\left(r\right)dr. \tag{B.7}$$

Hence, equation (B.6) becomes:

$$\frac{d^{\beta}\overline{\overline{T}}_{mp}^{\varphi}}{dt^{\beta}}+\kappa_1\gamma_{1mp}^2\overline{\overline{T}}_{mp}^{\varphi}=\sum_{i=1}^{k}\left[rR_{imp}\left(r\right)\frac{\partial\overline{\overline{T}}_{im}}{\partial r}-r\overline{\overline{T}}_{im}\frac{\partial R_{imp}\left(r\right)}{\partial r}\right]_{r_{i-1}}^{r_i}+\overline{\overline{Q}}_{mp}^{\varphi}. \tag{B.8}$$

Using the interface conditions, we obtain the final equation:

$$\frac{d^{\beta}\overline{\overline{T}}_{mp}^{\varphi}}{dt^{\beta}}+A_2\overline{\overline{T}}_{mp}^{\varphi}=A_3\exp(at)+A_4\delta\left(t\right), \tag{B.9}$$

where: $A_2=q_2\left(\kappa_1/P_1\kappa_i\right)\gamma_{1mp}^2,\quad A_3=q_1A_1\left(\lambda_k r_k/\rho_k\right),\quad A_4=q_1A_1\int_{r_{i-1}}^{r_i}\left[\delta\left(r-r_a\right)\delta\left(t\right)rR_i\left(r\right)dr\right].$

Appendix C

The Fourier series expansion of $\overline{\overline{T}}_{im}\left(r,t\right)$ is given by:

$$\overline{\overline{T}}_{im}\left(r,t\right)=\sum_{p=1}^{\infty}c_{mp}\left(t\right)R_{imp}\left(r\right), \tag{C.1}$$

where: $c_{mp}\left(t\right)=\left[\sum_{i=1}^{k}P_1\int_{r_{i-1}}^{r_i}rR_{imp}\left(r\right)\overline{\overline{T}}_{im}dr\right]/\left[R_{imp}\left(\gamma_{imp}\right)\right].$

Now using equation (B.7) from Appendix-B, we get:

$$c_{mp}(t)=\left[\overline{\overline{T}}^{\varphi}_{mp}\right]/\left[R_{imp}\left(\gamma_{imp}\right)\right].$$

As per [36] and [37] this is valid for $\overline{T}_{i0}(r,t),\overline{T}_{imc}(r,t),\overline{T}_{ims}(r,t)$), leading to the following temperature equation:

$$\overline{T}_i(r,\theta,t)=\overline{T}_{i0}(r,t)+\sum_{m=1}^{\infty}\overline{T}_{imc}(r,t)\cos(m\theta)+\sum_{m=1}^{\infty}\overline{T}_{ims}(r,t)\sin(m\theta). \tag{C.2}$$

Using equation (C.1) in (C.2), we obtain:

$$\overline{T}_i(r,\theta,t)=\sum_{p=1}^{\infty}B_1R_{i0p}(r)+\sum_{m=1}^{\infty}\sum_{p=1}^{\infty}B_2R_{imp}(r)\cos(m\theta)+\sum_{m=1}^{\infty}\sum_{p=1}^{\infty}B_3R_{imp}(r)\sin(m\theta) \tag{C.3}$$

where: $$B_1=\left[\overline{\overline{T}}^{\varphi}_{0p}\right]/\left[R_{i0p}\left(\gamma_{i0p}\right)\right],B_2=\left[\overline{\overline{T}}^{\varphi}_{mpc}\right]/\left[R_{imp}\left(\gamma_{imp}\right)\right],B_3=\left[\overline{\overline{T}}^{\varphi}_{mps}\right]/\left[R_{imp}\left(\gamma_{imp}\right)\right].$$

Using Fourier sine inversion on equation (C2), the final temperature distribution is:

$$\begin{aligned}T_i(r,z,\theta,t)=&\sum_{n=1}^{\infty}\{\sum_{p=1}^{\infty}B_1R_{i0p}(r)+\sum_{m=1}^{\infty}\sum_{p=1}^{\infty}B_2R_{imp}(r)\cos(m\theta)+\\&+\sum_{m=1}^{\infty}\sum_{p=1}^{\infty}B_3R_{imp}(r)\sin(m\theta)\}\sin(n\pi z/h).\end{aligned} \tag{C.4}$$

References

[1] Manthena V.R., Lamba N.K. and Kedar G.D. (2018): *Estimation of thermoelastic state of a thermally sensitive functionally graded thick hollow cylinder: a mathematical model*.– Journal of Solid Mechanics, vol.10, No.4, pp.766-778.

[2] Manthena V.R., Lamba N.K. and Kedar G.D. (2018): *Mathematical modeling of thermoelastic state of a thick hollow cylinder with nonhomogeneous material properties*.– Journal of Solid Mechanics, vol.10, No.1, pp.142-156.

[3] Manthena V.R. and Kedar G.D. (2019): *On thermoelastic problem of a thermosensitive functionally graded rectangular plate with instantaneous point heat source*.– Journal of Thermal Stresses, vol.42, No.7, pp.849-862, https://doi.org/10.1080/01495739.2019.1587327.

[4] Abouelregal A., Atta D. and Sedighi H.M. (2023): *Vibrational behavior of thermoelastic rotating nanobeams with variable thermal properties based on memory-dependent derivative of heat conduction model*.– Archive of Applied Mechanics, vol.93, pp.197-220, https://doi.org/10.1007/s00419-022-02110-8.

[5] Atta D. (2022): *Thermal diffusion responses in an infinite medium with a spherical cavity using the Atangana-Baleanu fractional operator*.– Journal of Applied and Computational Mechanics, vol.8, pp.1358-1369, https://doi.org/10.22055/jacm.2022.40318.3556.

[6] Lamba N.K. (2022): *Thermosensitive response of a functionally graded cylinder with fractional order derivative*.– International Journal of Applied Mechanics and Engineering, vol.27, No.1, pp.107-124, https://doi.org/10.2478/ijame-2022-0008.

[7] Abouelregal A.E., Sofiyev A.H., Sedighi H.M. and Fahmy M.A. (2023): *Generalized heat equation with the Caputo-Fabrizio fractional derivative for a nonsimple thermoelastic cylinder with temperature-dependent properties*.– Physical Mesomechanics, vol.26, No.2, pp.224-240, https://doi.org/10.1134/S1029959923020108.

[8] Khavale S.G. and Gaikwad K.R. (2023): *Fractional ordered thermoelastic stress analysis of a thin circular plate under axi-symmetric heat supply*.– International Journal of Nonlinear Analysis and Applications, vol.14, No.4, pp.207-219, https://doi.org/10.22075/ijnaa.2023.29131.4067.

[9] Lamba N.K. (2023): *Impact of memory-dependent response of a thermoelastic thick solid cylinder*.– Journal of Applied and Computational Mechanics, vol.9, No.4, pp.1135-1143, https://doi.org/10.22055/jacm.2023.43952.4149.

[10] Lamba N.K., Verma J. and Deshmukh K. (2023): *A brief note on space time fractional order thermoelastic response in a layer*.– App. and Appl. Mathem., vol.18, No.1, pp.1-9, https://digitalcommons.pvamu.edu/aam/vol18/iss1/18.

[11] Saidi A., Yahya A.M.H., Abouelregal A.E., Dargail H.E., Ahmed I.E., Ali E. and Mohammed F.A. (2023): *Generalized thermoelastic heat conduction model involving three different fractional operators*.– Advances in Materials Science, vol.23, No.2, pp.25-44, https://doi.org/10.2478/adms-2023-0009.

[12] Singh B. (2023): *Wave propagation in different theories of fractional thermoelasticity*.– Journal of Engineering and Thermal Sciences, vol.3, No.1, pp.1-10, https://doi.org/10.21595/jets.2023.23067.

[13] Tian L., Peng W. and He T. (2023): *A modified fractional-order thermo-viscoelastic model and its application in thermal-induced nonlocal response analysis of a microscale plate*.– Archive of Applied Mechanics, vol.93, No.2, pp.687-705, https://doi.org/10.1007/s00419-022-02293-0.

[14] Wang Y.W., Chen J., Zheng R.Y. and Li X.F. (2023): *Thermoelastic damping in circular microplate resonators based on fractional dual-phase-lag model and couple stress theory*.– International Journal of Heat and Mass Transfer, vol.201, 123570, https://doi.org/10.1016/j.ijheatmasstransfer.2022.123570.

[15] Abouelregal A.E., Marin M., Askar S.S. and Foul A. (2024): *Transient thermoelastic response in a semi-infinite medium subjected to a moving heat source: an implementation of the Moore-Gibson-Thompson model with higher-order memory-dependent derivatives*.– Mechanics of Time-Dependent Materials, vol.28, No.3, pp.1555-1581, https://doi.org/10.1007/s11043-024-09672-w.

[16] Guo Y., Xiong C., Yu W., Li J., Ma J. and Du C. (2024): *Coupling dynamic response of saturated soil with anisotropic thermal conductivity under fractional order thermoelastic theory*.– PLOS ONE, vol.19, No.4, e0297651, https://doi.org/10.1371/journal.pone.0297651.

[17] Jamal M., Bibi F., Azhar E. and Ali H. (2024): *Investigating reflection phenomenon of plane waves in a fractional order thermoelastic rotating medium using nonlocal theory*.– Mechanics of Time-Dependent Materials, vol.28, No.3, pp.1375-1393, https://doi.org/10.1007/s11043-024-09709-0.

[18] Khader S.E., Marrouf A.A. and Khedr M. (2024): *Application of the fractional-order theory of micropolar thermoelasticity in the solid cylinder*.– Journal of the Brazilian Society of Mechanical Sciences and Engineering, vol.46, No.8, 459, https://doi.org/10.1007/s40430-024-04941-8.

[19] Li C., Liu J. and He T. (2024): *Fractional-order rate-dependent thermoelastic diffusion theory based on new definitions of fractional derivatives with non-singular kernels and the associated structural transient dynamic responses analysis of sandwich-like composite laminates*.– Communications in Nonlinear Science and Numerical Simulation, vol.132, 107896, https://doi.org/10.1016/j.cnsns.2024.107896.

[20] Li Y., Li Y., Han Y. and Wang C. (2024): *Propagation of coupled waves across a magneto-electro-thermo-elastic interface with consideration of fractional order thermoelasticity and microstructural effect*.– Acta Mechanica, vol.235, No.9, pp.1-20, https://doi.org/10.1007/s00707-024-04000-2.

[21] Li Y., Wei P., Zhang P. and Gao X. (2024): *Thermoelastic wave and thermal shock based on dipolar gradient elasticity and fractional-order generalized thermoelasticity*.– Waves in Random and Complex Media, vol.34, No.3, pp.1226-1250, https://doi.org/10.1080/17455030.2021.1933258.

[22] Liu F., Shi P. and Guo Y. (2024): *The thermoelastic dynamic response of a rod due to a moving heat source under the fractional-order thermoelasticity theory*.– Symmetry, vol.16, 666, https://doi.org/10.3390/sym16060666.

[23] Manthena V.R., Srinivas V.B., Lamba N.K. and Kedar G.D. (2024): *Fractional thermal response in a thermosensitive rectangular plate due to the action of a moving source of heat*.– Advances in Differential Equations and Control Processes, vol.31, No.3, pp.397-415, https://doi.org/10.17654/0974324324022.

[24] Tiwari R., Abouelregal A.E., Shivay O.N. and Megahid S.F. (2024): *Thermoelastic vibrations in electro-mechanical resonators based on rotating microbeams exposed to laser heat under generalized thermoelasticity with three relaxation times*.– Mechanics of Time-Dependent Materials, vol.28, pp.423-447, https://doi.org/10.1007/s11043-022-09578-5.

[25] Zhao L., Wei P. and Li Y. (2024): *Dynamic behavior of nanoplate on viscoelastic foundation based on spatial-temporal fractional order viscoelasticity and thermoelasticity*.– European Journal of Mechanics - A Solids, vol.103, 105179, https://doi.org/10.1016/j.euromechsol.2023.105179.

[26] Abbas I.A. (2015): *Generalized thermoelastic interaction in functional graded material with fractional order three-phase lag heat transfer*.– Journal of Central South University, vol.22, pp.1606-1613, https://doi.org/10.1007/s11771-015-2677-5.

[27] Abbas I., Saeed T. and Alhothuali M. (2021): *Hyperbolic two-temperature photo-thermal interaction in a semiconductor medium with a cylindrical cavity*.– Silicon, vol.13, pp.1871-1878, https://doi.org/10.1007/s12633-020-00570-7.

[28] Alzahrani F.S. and Abbas I.A. (2020): *Photo-thermal interactions in a semiconducting media with a spherical cavity under hyperbolic two-temperature model*.– Mathematics, vol.8, No.4, 585, https://doi.org/10.3390/math8040585.

[29] Abbas I.A. and Othman M.I.A. (2012): *Plane waves in generalized thermo-microstretch elastic solid with thermal relaxation using finite element method*.– International Journal of Thermophysics, vol.33, pp.2407-2423, https://doi.org/10.1007/s10765-012-1340-8.

[30] Carrera E., Abouelregal A.E., Abbas I.A. and Zenkour A.M. (2015): *Vibrational analysis for an axially moving microbeam with two temperatures*.– Journal of Thermal Stresses, vol.38, No.6, pp.569-590, https://doi.org/10.1080/01495739.2015.1030635.

[31] Ozisik M.N. (1984): *Heat Transfer: A Basic Approach*.– McGraw Hill Publications, New York.

[32] Caputo M. (1967): *Linear models of dissipation whose Q is almost frequency independent–II*.– Geophysical Journal International, vol.13, pp.529-539, https://doi.org/10.1111/j.1365-246X.1967.tb02303.x.

[33] Caputo M. and Mainardi F. (1971): *Linear models of dissipation in anelastic solids*.– La Rivista del Nuovo Cimento, vol.1, pp.161-198, https://doi.org/10.1007/BF02820620.

[34] Eringen A.C. (1974): *Theory of nonlocal thermoelasticity*.– International Journal of Engineering Science, vol.12, No.12, pp.1063-1077, https://doi.org/10.1016/0020-7225(74)90033-0.

[35] Singh S., Jain P.K. and Rizwan-uddin (2011): *Finite integral transform method to solve asymmetric heat conduction in a multilayer annulus with time-dependent boundary conditions*.– Nuclear Engineering and Design, vol.241, pp.144-154, https://doi.org/10.1016/j.nucengdes.2010.10.010.

[36] Manthena V.R., Srinivas V.B. and Kedar G.D. (2020): *Analytical solution of heat conduction of a multilayered annular disc and associated thermal deflection and thermal stresses*.– Journal of Thermal Stresses, vol.43, No.5, pp.563-578, https://doi.org/10.1080/01495739.2020.1735975.

[37] Noda N., Hetnarski R.B. and Tanigawa Y. (2003): *Thermal Stresses*.– 2nd edition, Taylor & Francis, New York.

[38] Nur Alam M., Abdur Rahim M., Najmul Hossain M. and Tunc C. (2024): *Dynamics of damped and undamped wave natures of the fractional Kraenkel-Manna-Merle system in ferromagnetic materials*.– Journal of Applied and Computational Mechanics, vol.10, No.2, pp.317-329, https://doi.org/10.22055/jacm.2023.45064.4307.

[39] Nadeem M., He J.H., He C.H., Sedighi H.M. and Shirazi A.H. (2022): *A numerical solution of nonlinear fractional Newell-Whitehead-Segel equation using natural transform*.– TWMS Journal of Applied and Engineering Mathematics, vol.13, No.2, pp.168-182.

[40] Verma S., Kulkarni V.S. and Deshmukh K.C. (2015): *Finite element solution to transient asymmetric heat conduction in multilayer annulus*.– International Journal of Advances in Applied Mathematics and Mechanics, vol.2, No.3, pp.119-125.

[41] Kulkarni V.S. and Deshmukh K.C. (2008): *Thermal stresses in a thick annular disc*.– Journal of Thermal Stresses, vol.31, No.4, pp.331-342, https://doi.org/10.1080/01495730701738325.

[42] Shariyat M. and Sedaghat A.M. (2023): *Generalized fractional-order hygro-thermo-viscoelastic wave propagation/reflection in annular spinning discs: comparisons with the classical and Lord-Shulman thermo-viscoelastic models*.– Journal of the Brazilian Society of Mechanical Sciences and Engineering, vol.45, No.10, 506, https://doi.org/10.1007/s40430-023-04430-y.

[43] Wange N.J., Dandale M.N. and Waikar V. (2023): *Analytical solution for fractional order temperature distribution in two dimensional multilayer composite circular discs*.– IOP Conference Series: Materials Science and Engineering, vol.1291, No.1, 012029, https://doi.org/10.1088/1757-899X/1291/1/012029.

[44] Lamba N.K., Manthena V.R., Bhad P.P., Srinivas V.B. and Abouelregal A.E. (2025): *Thermal characteristics of a multilayered annular disk with thermosensitive features using a fractional-order heat conduction model*.– Acta Mechanica, vol.236, pp.937-958, https://doi.org/10.1007/s00707-024-04172-8.

[45] Eroğlu M., Esen İ. and Koç M.A. (2025): *The effect of an auxetic core layer and symmetric FGM face layers on the 3D wave propagation response of sandwich nanoplates*.– Archive of Applied Mechanics, vol.95, https://doi.org/10.1007/s00419-025-02772-0.

[46] Abouelregal A.E., Akgöz B. and Civalek Ö. (2023): *Magneto-thermoelastic interactions in an unbounded orthotropic viscoelastic solid under the Hall current effect by the fourth-order Moore-Gibson-Thompson equation*.– Computers & Mathematics with Applications, vol.141, pp.102-115, https://doi.org/10.1016/j.camwa.2023.03.032.

[47] Civalek O. and Jalaei M.H. (2020): *Shear buckling analysis of functionally graded (FG) carbon nanotube reinforced skew plates with different boundary conditions*.– Aerospace Science and Technology, vol.99, 105753, https://doi.org/10.1016/j.ast.2020.105753.

[48] Civalek Ö. and Demir C. (2011): *Buckling and bending analyses of cantilever carbon nanotubes using the Euler-Bernoulli beam theory based on non-local continuum model*.– Asian Journal of Civil Engineering, vol.12, No.5, pp.651-661.

[49] Warbhe S.D. and Gujarkar V. (2025): *Thermoelastic behavior of a hollow cylinder using space-time fractional heat conduction: a quasi-static approach*.– International Journal of Applied Mechanics and Engineering, vol.30, No.4, pp.153-164, DOI: https://doi.org/10.59441/ijame/210537.

[50] Dastjerdi S., Naeijian F., Akgöz B. and Civalek Ö. (2021): *On the mechanical analysis of microcrystalline cellulose sheets*.– International Journal of Engineering Science, vol.166, 103500, https://doi.org/10.1016/j.ijengsci.2021.103500.

[51] Abouelregal A.E., Bekir Akgöz B. and Civalek Ö. (2022): *Nonlocal thermoelastic vibration of a solid medium subjected to a pulsed heat flux via Caputo-Fabrizio fractional derivative heat conduction*.– Applied Physics A, vol.128, No.660.

[52] Ailawalia P., Falicki J. and Salhotra S. (2025): *Anti-plane deformation in Green-Naghdi (Type III) thermoelastic medium*.– International Journal of Applied Mechanics and Engineering, vol.30, No.3, pp.1-10, DOI: https://doi.org/10.59441/ijame/205462.a

Received: February 19, 2026

Revised: June 2, 2026